3D AVO crossplotting—An effective visualization technique

SATINDER CHOPRA, VLADIMIR ALEXEEV, and YONG XU, Core Laboratories Reservoir Technologies Division, Calgary, Alberta, Canada

Crossplots, visual representations of the relationship between two variables, are used to (a) visually identify outliers that may bias a correlation, (b) gain a visual sense for the strength of the correlation between variables, (c) detect if the relationship between variables is linear or nonlinear, (d) identify trends which may indicate multiple populations within the same data set, and (e) detect significant departures from a background trend—in other words to detect anomalies.

Crossplotting is widely used in AVO analysis, because it facilitates the simultaneous and meaningful evaluation of two attributes. Generally, common lithology units and fluid types cluster together in AVO crossplot space, allowing identification of background lithology trends and anomalous off-trend aggregations that could be associated with hydrocarbons.

Initially, AVO crossplotting typically used the intercept and gradient. However, in 1997, Goodway et al. used crossplots of elastic parameters (Lambda-Rho and Mu-Rho) to improve petrophysical discrimination of rock properties. Other attributes have also been used as AVO anomaly indicators (Castagna and Smith, 1994). Crossplotting appropriate pairs of attributes so that common lithologies and fluid types generally cluster together allows for straightforward interpretation. The off-trend aggregations can then be more elaborately evaluated as potential hydrocarbon indicators. This is the essence of successful AVO crossplot analysis and interpretation, all of which is based on the premise that data that are anomalous statistically are interesting geologically.

This article describes attempts to extend crossplotting to three dimensions and assess any advantages that result. Ross and Sparlin (2000) made this extension by using the intercept, gradient, and inlines for a 3D seismic volume as the three dimensions on a 3D crossplot.

Our procedure begins by first visualizing different combinations of the measured well-log parameters (P-velocity, S-velocity, density, porosity, and gamma ray) in two and three dimensions. Next, observed patterns are visualized and compared in the derived parameter crossplot space. The data sets have different lithologic depositions and areas. This analysis is then extended to 3D crossplot space for both well log and 3D seismic data. However, a variety of parameters are used on the various axes.

In our view, data clusters "hanging in 3D space" are more readily diagnostic, resulting in more accurate and reliable interpretation.

The examples discussed here have been selected not as outstanding solutions to problems but to demonstrate the advantages of 3D crossplotting when probing complex subsurface intervals.

Example 1. The first example is a Mississippian-age organic-rich shale that is the reservoir for the Barnett Shale unconventional gas accumulation in the Fort Worth Basin, one of the most active areas in Texas. Production from Barnett Shale comes from fractures that appear controlled by physical and chemical means. It is believed that hydrocarbon generation resulted in volume expansion of the source rock that eventually led to microfractures. Tectonic forces helped form bigger fractures that increased their overall extent. In some cases this weakened the self-sealing nature of these shale petroleum systems.

Figure 1a shows the velocity log from a well from this area. Traditional well log evaluation—i.e., comparing the different curves—has proved a poor method of predicting production from the Barnett Shale. So, we decided to try 3D AVO visualization and loaded the available suite of logs into software that has 2D/3D crossplotting features for both well log and seismic data and their derived attributes.

In Figure 1b, a simple crossplot of the V_P and V_S curves of the well log, the different formation tops (marked on the velocity curve) correspond to at least four limestone layers, two sandstone layers, and five shale layers. Gas is being produced from the fifth shale layer which is just above the Base of Shale marker in Figure 1a and overlain by impermeable limestone 4 layer that serves as a "frac" barrier. The two sandstone layers and the four unproductive shale layers were assigned the same colors (purple and blue, respectively); the productive shale is yellow. The four limestone layers were assigned different colors. Figure 1b clearly distinguishes the sandstone cluster, the limestone cluster, and the Barnett Shale "sweet spot" which shows a distinct linear trend with a curved sliver at its lower side.

By drawing a polygon around each of these clusters (Figure 1c), one can mark the log zones from which these data points originated. Clearly, for the sweet spot, the linear trend represents the producing Barnett Shale and the curved sliver comes from a narrow interval where the velocity just begins to decrease.

Convincing cluster patterns can also be seen in the derived elastic parameter crossplot space. Figure 1d shows a crossplot of Lambda Rho versus Mu Rho. Lambda-Rho is a sensitive indicator of water versus gas saturation and Mu-Rho is used to help determine pure rock fabric or lithology. In this case, the different clusters are more separated in this crossplot than in the V_P versus V_S crossplot.

It is possible to add a third dimension to any of these crossplots by adding a density axis, a porosity axis, or a gamma-ray axis. Figures 2a and 2b show 3D crossplots, one with density as the third axis and the other with gamma ray. Two useful observations emerge:

- In the Lambda Rho versus Lambda Mu crossplot, the carbonate cluster includes the four different layers of limestone. However, as the 3D crossplot cube is turned about the vertical axis, the density of limestone layer 1 is not as high as the other layers, and density varies in this layer. This could imply that limestone layer 1, instead of being one layer, could possibly be a combination of two sublayers with different densities (an indication to this effect is seen in Figure 1a).
- The curved layer that is linked to the gas-producing Barnett Shale cluster may not represent a part of it; as seen in Figure 2b, while the linear trend is seen associated with

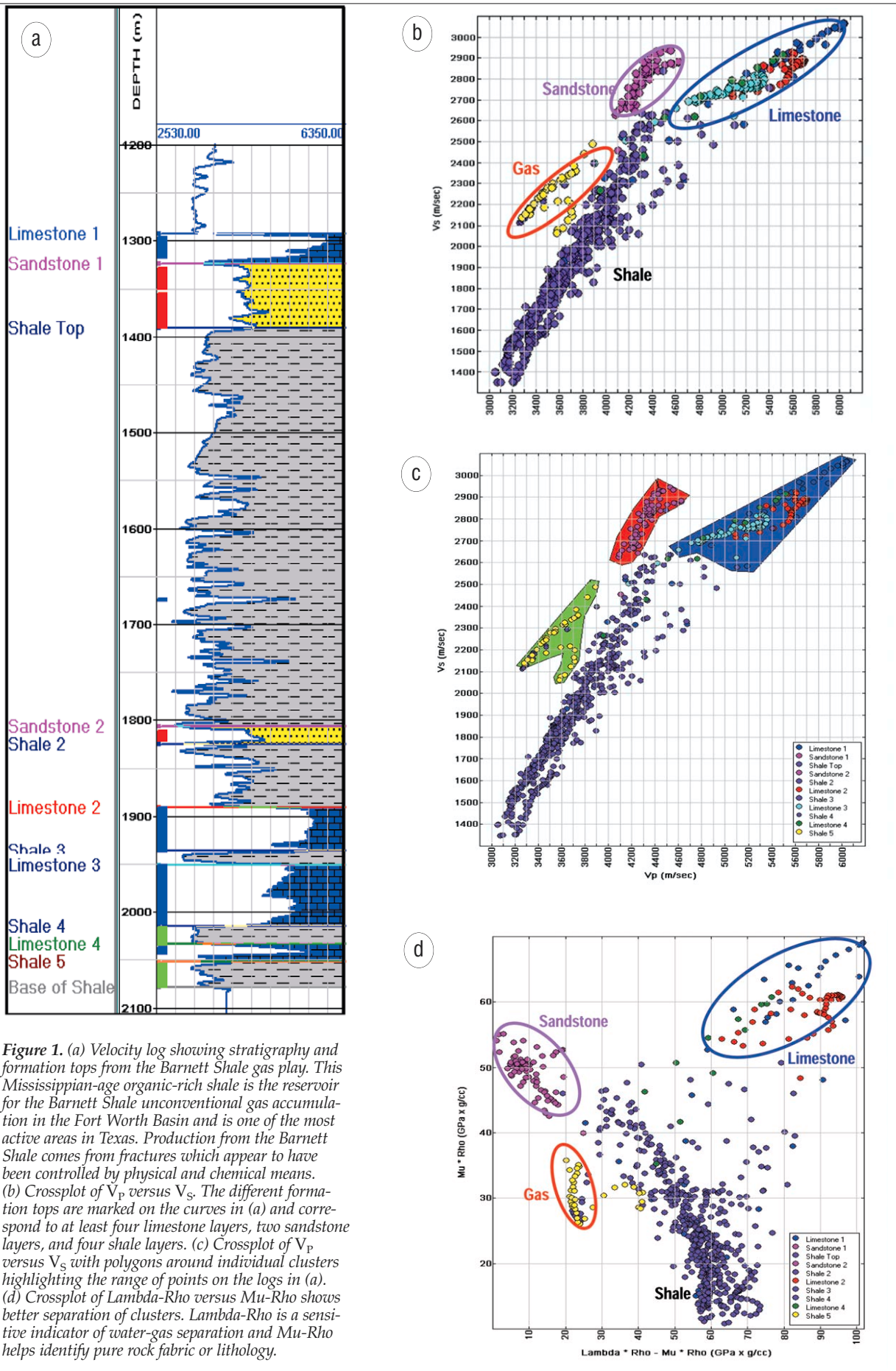

Figure 1. *(a) Velocity log showing stratigraphy and formation tops from the Barnett Shale gas play. This Mississippian-age organic-rich shale is the reservoir for the Barnett Shale unconventional gas accumulation in the Fort Worth Basin and is one of the most active areas in Texas. Production from the Barnett Shale comes from fractures which appear to have been controlled by physical and chemical means. (b) Crossplot of V_P versus V_S. The different formation tops are marked on the curves in (a) and correspond to at least four limestone layers, two sandstone layers, and four shale layers. (c) Crossplot of V_P versus V_S with polygons around individual clusters highlighting the range of points on the logs in (a). (d) Crossplot of Lambda-Rho versus Mu-Rho shows better separation of clusters. Lambda-Rho is a sensitive indicator of water-gas separation and Mu-Rho helps identify pure rock fabric or lithology.*

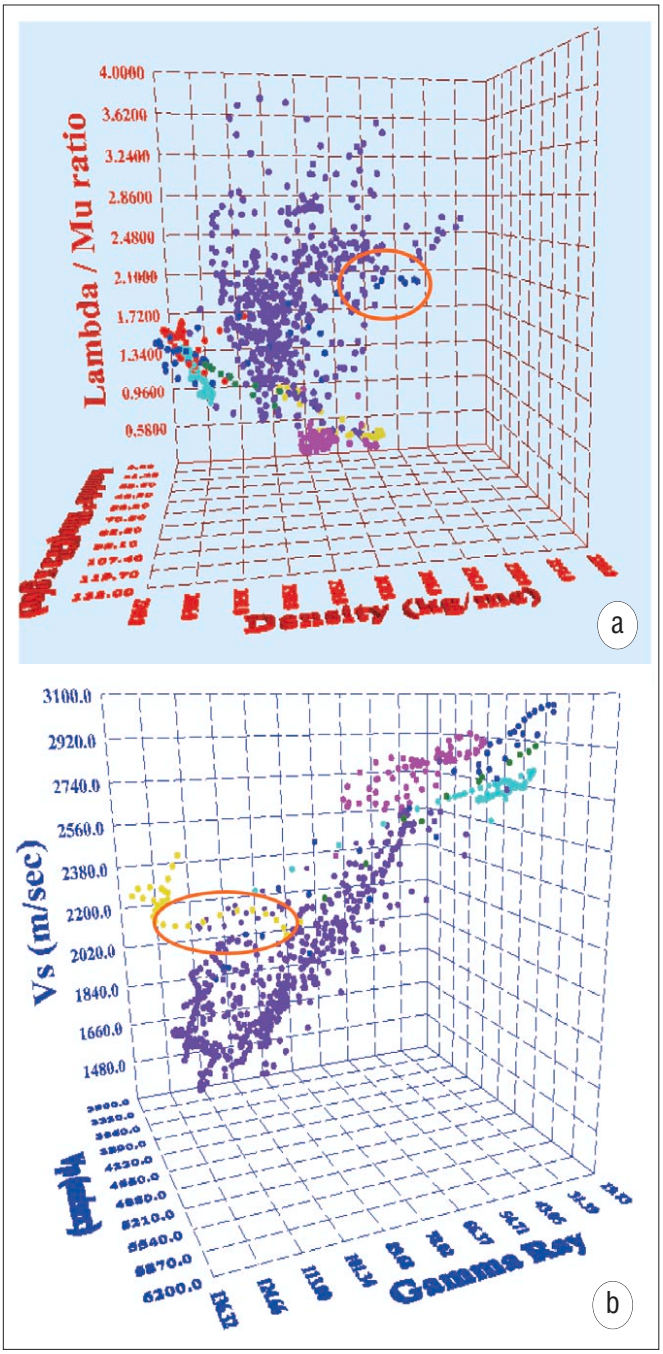

Figure 2. *(a) 3D plot of Lambda-Rho, Lambda/Mu, and density. (b) 3D plot of* V_P, V_S, *and gamma ray. Such a crossplot allows simultaneous interpretation of the three attributes. Individual clusters can be studied by simply turning the cube from one side to the other.*

high gamma-ray values, the curved sliver shows a gradual variation in these values which extends over at least 40 API units (red ellipse).

We feel this demonstrates that interactively examining all available and derived curves in 3D crossplot space enables the interpreter to better understand the lithological layering in the subsurface and better assess hydrocarbon-bearing zones or key lithologies.

Example 2. Electrical resistivity and sonic logs are usually used to identify gas hydrates because, in contrast to water-saturated sediments, gas-hydrate-bearing sediments exhibit anomalously high electrical resistivities and high acoustic velocities. The solid nature of gas hydrates is more supportive of seismic wave propagation (particularly P-wave propagation). Therefore, the compressional velocity in gas-hydrate-bearing sediments is usually several times higher than that in gas-bearing sediments.

Consequently, at the base of the gas-hydrate stability zone (the contact between gas-hydrate and free-gas-bearing sediments), the sonic log shows a distinct drop in acoustic velocity.

The Mallik 2L-38 gas hydrate research well was drilled by JAPEX/JNOX/GSC in early 1998 to a depth of 1150 m. The base of the methane hydrate stability zone, predicted from borehole temperature surveys, is 1100 m. Borehole electrical resistivity and acoustic velocity (both P and S) logs confirm in-situ gas hydrates between 888.84 and 1102.2 m. Deep electrical resistivity measurements range from 10 to 50 ohm-m, compressional wave velocity from 2.5 to 3.6 km/s, and shear wave velocity from 1.1 to 2.0 km/s. In 3D crossplot space (Figure 3), by choosing any of these parameters, it is possible to visualize the anomalous cluster patterns and make the necessary inferences. The hydrate layers have large resistivities (depending on their saturation) and smaller gamma-ray values (depending on the lithology).

Interactive 3D AVO attribute crossplotting. Interactive 3D crossplotting is computationally intensive. An area of 100 km^2 with a 500-ms time window at 2 ms sample rate and a square bin of 25 m will generate 40 million pairs. A 3D volume with 200 inlines and 200 crosslines, 500-ms segmented window, 2-ms sample interval, and a square bin of 25 m involves 10 million pairs. While it is possible to load this amount of data, the extreme density of the individual points may complicate extraction of meaningful information. It is, of course, possible to load subvolumes that encompass the anomalies of interest; but, for a data set to be efficiently visualized, suitable decimation (every alternate inline or crossline or any other increment) may also be required apart from segmentation (suitable time window). Figure 4 shows an example from a producing Cretaceous-aged gas field in southern Alberta. At least three sand-bearing channels can be interpreted on a composite plot where high amplitude envelope values are overlayed on a coherence slice (Figure 4a). This has independently been confirmed by Lambda-Rho and Mu-Rho analysis (Pruden, 2002). Figure 4b shows a 3D crossplot for the anomaly on the right in Figure 4a. Twenty-one complete inlines (10 on each side of the blue line in Figure 4a) have been selected and 200 ms of the data in the zone of interest Lambda-Rho and Mu-Rho volumes have been used for generating this crossplot. Lambda-Rho, Mu-Rho, and inlines are the three axes in Figure 4b. The cluster of points is shaded in three colors—bright red, purple, and blue. Clearly, the red cluster of points within the yellow ring corresponds to the anomaly. As the 3D crossplot is turned to one side, the bright red cluster is seen to extend over a certain patch of inlines and this areal spread of the red cluster indicates the extent of the anomaly.

While this 3D crossplot gives a visual sense about the areal spread of the anomaly in Lambda-Rho versus Mu-Rho crossplot space, one could argue that it is essentially a series of 2D Lambda-Rho versus Mu-Rho crossplots stacked together—one for each of the 21 inlines. This prompted us to choose different parameters for the three axes of the 3D crossplot. The combination of parameters chosen should then enable a convenient and meaningful deciphering of anomalous clusters in 3D crossplot space. Lambda-Rho, Mu-Rho, and fluid stack could be one such combination. Fluid stack highlights zones where P-reflectivity differs from

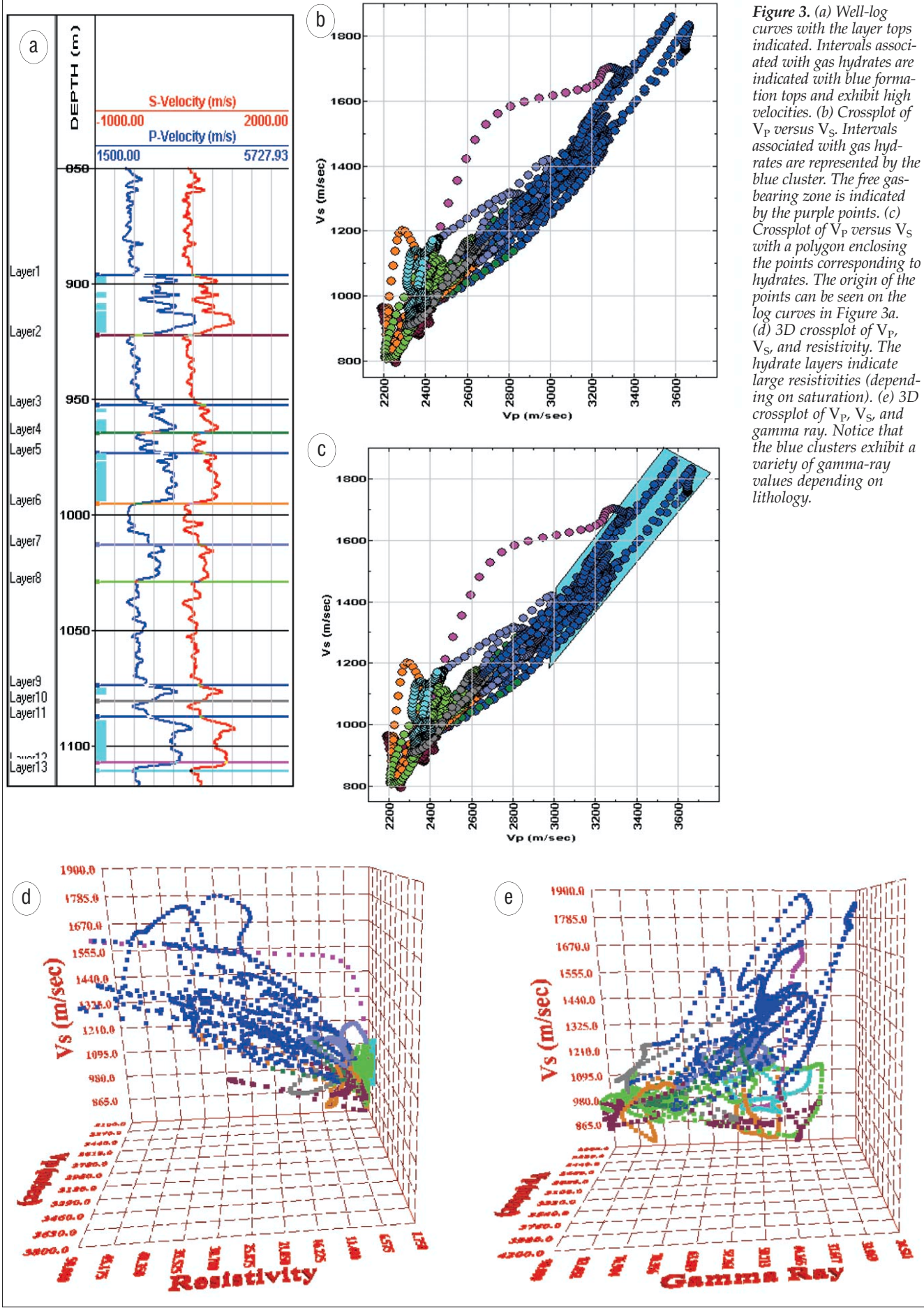

Figure 3. *(a) Well-log curves with the layer tops indicated. Intervals associated with gas hydrates are indicated with blue formation tops and exhibit high velocities. (b) Crossplot of V_P versus V_S. Intervals associated with gas hydrates are represented by the blue cluster. The free gas-bearing zone is indicated by the purple points. (c) Crossplot of V_P versus V_S with a polygon enclosing the points corresponding to hydrates. The origin of the points can be seen on the log curves in Figure 3a. (d) 3D crossplot of V_P, V_S, and resistivity. The hydrate layers indicate large resistivities (depending on saturation). (e) 3D crossplot of V_P, V_S, and gamma ray. Notice that the blue clusters exhibit a variety of gamma-ray values depending on lithology.*

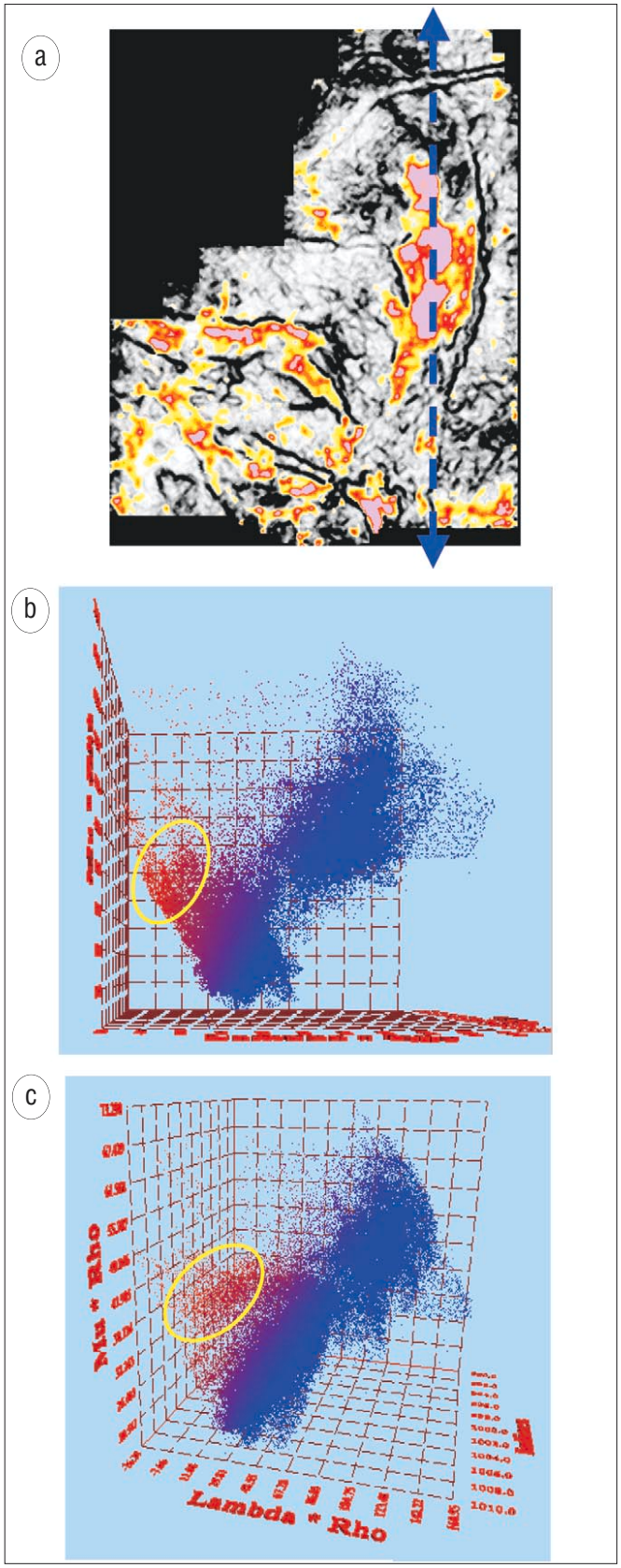

Figure 4. *(a) Composite display of reservoir channel sands. While the boundaries of the channels are distinct on the coherence slice, the high-amplitude envelope values indicate sandstone deposition. This is independently confirmed by Lambda-Mu-Rho analysis. (b) 3D crossplot for Lambda-Rho-Mu-Rho inlines, seen facing the Lambda-Rho and Mu-Rho axes. The anomaly corresponding to the channel reservoir sands is bright red (low Lambda-Rho and high Mu-Rho). (c) As this crossplot is turned, the extent of the anomaly becomes clearer.*

S-reflectivity. For gas bearing zones the P-reflectivity will be different (lower) from the S-reflectivity. A gas sand, for example, would exhibit low values of Lambda-Rho, high values of Mu-Rho, and negative values of fluid stack.

Figure 5 shows these three indicators crossplotted for a gas anomaly—Lambda-Rho on the x-axis, Mu-Rho on the y-axis and fluid stack on the z-axis. On Figure 5a, a time slice from a Lambda-Rho volume, the gas anomaly is indicated by the blue patch. A polygon (red) is drawn to select the live data points on the time slice that can be brought into the crossplot. The red cluster of points in Figure 5b comes from this red polygon and five time slices (two above and two below the one shown). As the crossplot is turned toward the left on the vertical axis, the fluid stack shows the expected negative values for the gas sand. It is possible that the clusters of points coming from outside the anomaly clutter the crossplot and may mask the points coming from the anomaly. A selection of points coming from any polygon can be incorporated into the software to allow the desired set of points to be displayed in the crossplot. As seen here, only points coming from the purple polygon (marked in Figure 5a) can be seen in Figure 5e.

Figure 6 shows a Lambda-Rho, Lambda/Mu, fluid stack 3D crossplot. A yellow polygon, corresponding to the prospective anomaly, drawn within a red polygon shows low values of Lambda-Rho and low values of Lambda-Mu (not shown), which are expected of a gas sand. Figures 6b and 6c show the spread of these low values (yellow) indicating negative values for fluid stack.

Figure 7 shows a time slice from the P-reflectivity (R_P) volume for the same data set used in Figures 4, 5, and 6. A yellow polygon marks the anomaly. The same polygon is assigned to the S-Reflectivity (R_S) and fluid stack time slices. On the 3D crossplot with axes for R_P, R_S, and fluid stack, the yellow polygon lights up a yellow cluster in a red background cluster. As the cube is turned, the fluid stack indicates these negative yellow values correspond to the anomaly.

Though not included in this analysis, an ideal combination of the three attributes would be Lambda-Mu-density. Distinction between highly porous, gassy oil versus lower porosity could be made on the Lambda axis, sand shale and silt clusters could be distinguished on the Mu axis, and porosity could be visualized on the density axis. For appropriate data, such a 3D crossplot would be very useful.

Conclusions. 3D AVO crossplots allow the interpreter to look at the disposition of individual clusters in a 3D cube that can be oriented in any direction to get a detailed understanding of their arrangement or distribution.

The 3D crossplotting visualization of LMR (Lambda-Mu-Rho) attributes enables the display of cluster distribution corresponding to different lithologies when properly color-coded. Such distributions are often not so apparent on 2D crossplots.

Suggested reading. "Principles of AVO crossplotting" by Castagna and Smith (*TLE*, 1997). "Comparison of AVO indicators: A modeling study" by Castagna and Swan (GEOPHYSICS, 1994). "Framework for AVO gradient and intercept interpretations" by Castagna et al. (GEOPHYSICS, 1998). "Scientific results from JAPEX/JNOC/GSC Mallik 2L-38 gas hydrate research well, Mackenzie Delta, Northwest Territories, Canada" by Dallimore et al. (*Geological Survey of Canada Bulletin*, 1999). "A closer look at hydrocarbon indicators" by Foster et al. (*SEG 1993 Expanded Abstracts*). "Another perspective on AVO crossplotting" by Foster et al. (*TLE*, 1997). "Improved AVO fluid detec-

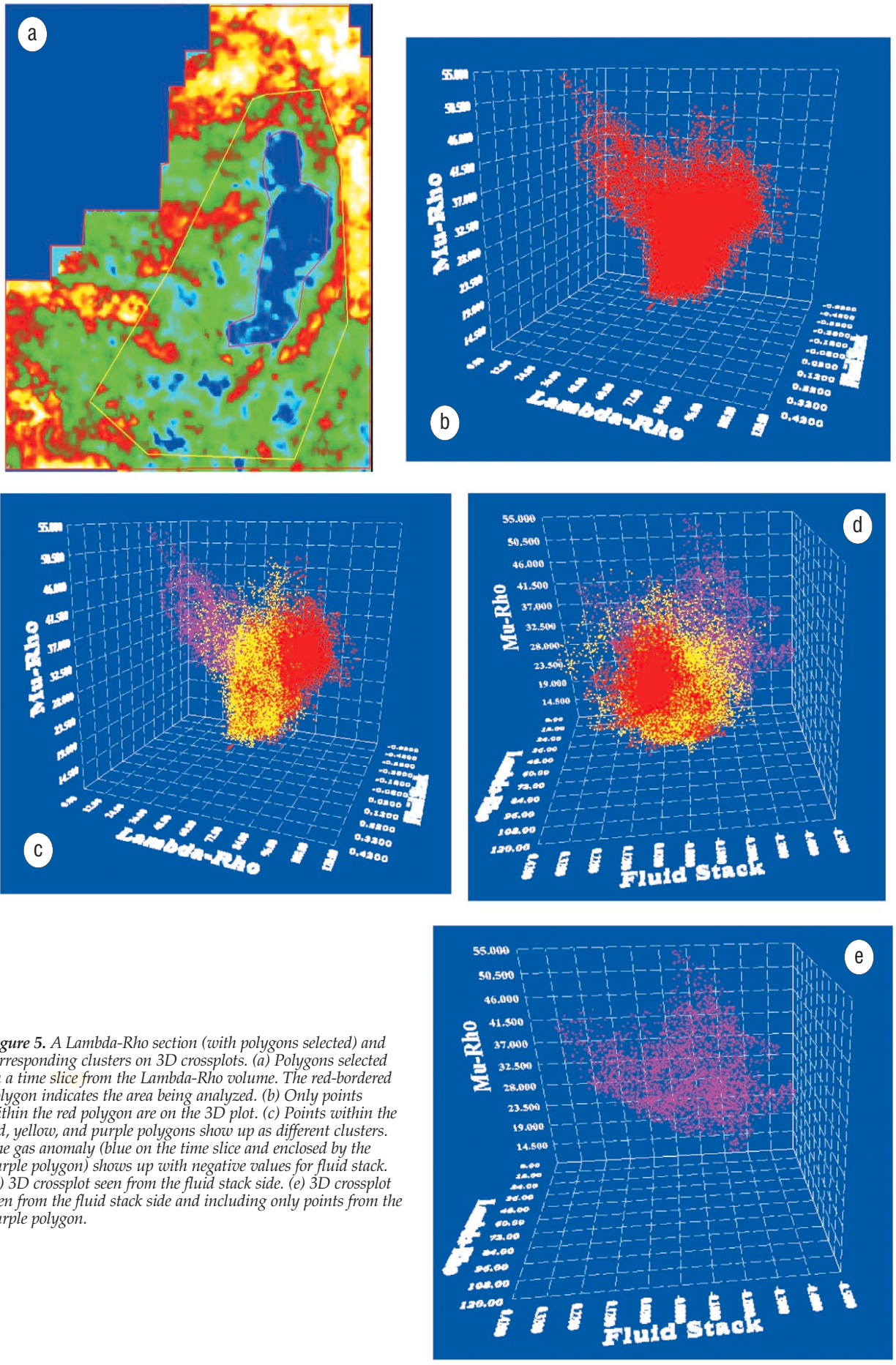

Figure 5. *A Lambda-Rho section (with polygons selected) and corresponding clusters on 3D crossplots. (a) Polygons selected on a time slice from the Lambda-Rho volume. The red-bordered polygon indicates the area being analyzed. (b) Only points within the red polygon are on the 3D plot. (c) Points within the red, yellow, and purple polygons show up as different clusters. The gas anomaly (blue on the time slice and enclosed by the purple polygon) shows up with negative values for fluid stack. (d) 3D crossplot seen from the fluid stack side. (e) 3D crossplot seen from the fluid stack side and including only points from the purple polygon.*

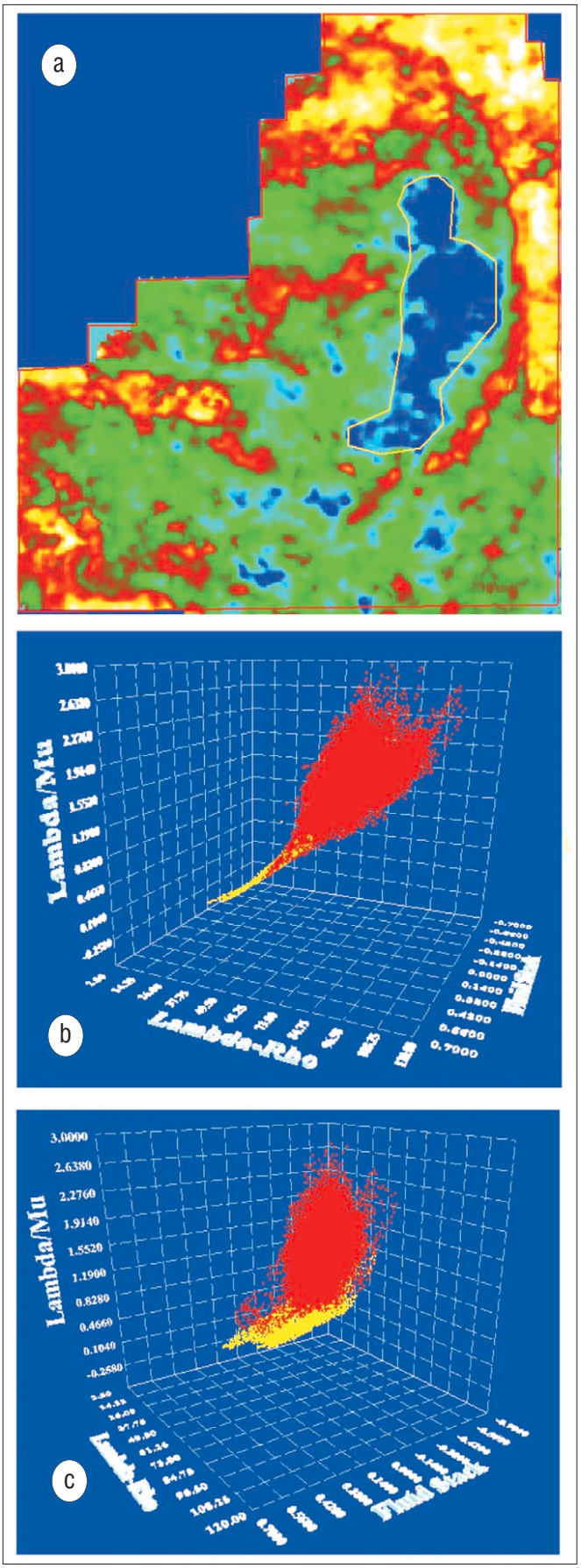

Figure 6. *3D crossplots for the polygons shown in (a) with Lambda-Rho, Lambda/Mu, and fluid stack as the three attributes. As expected, the gas anomaly enclosed in yellow exhibits low values of Lambda-Rho, low values of Lambda/Mu, and negative values of fluid stack.*

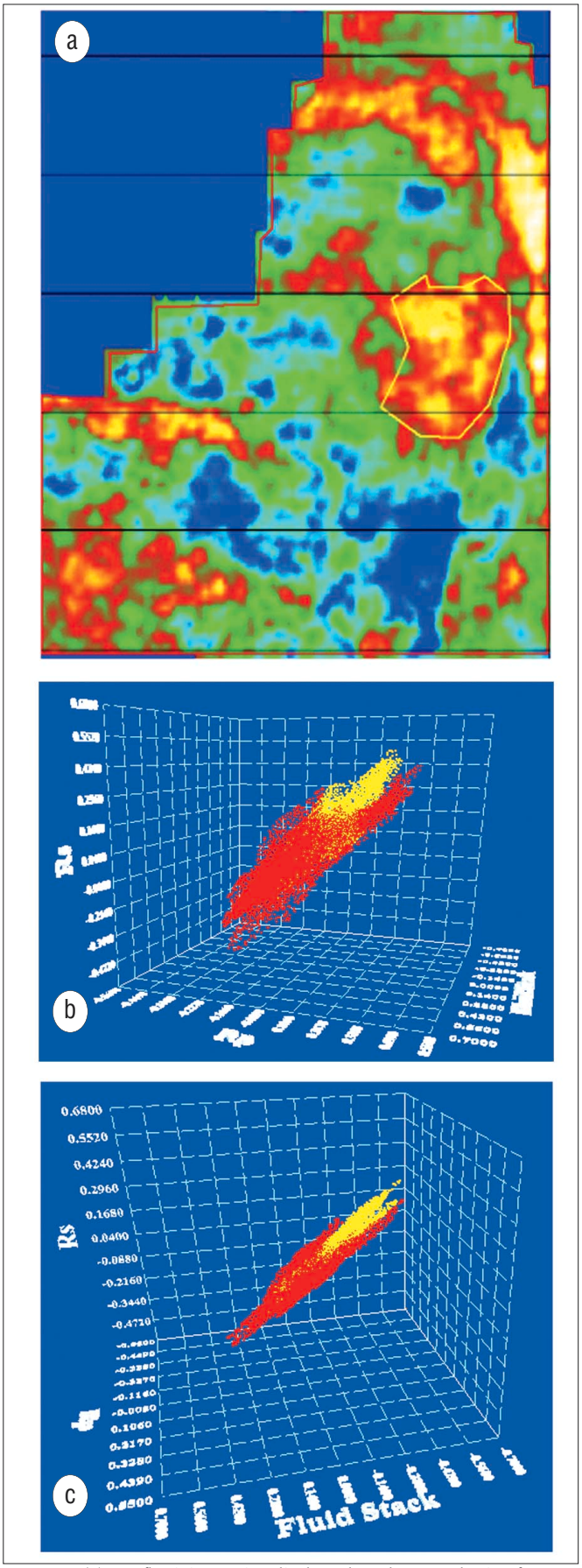

Figure 7. *(a) P-reflectivity section displays the polygons selection for 3D plotting. In (b) and (c), the yellow polygon enclosing the gas anomaly highlights, as expected, negative values of fluid stack.*

tion and lithology discrimination using Lamé petrophysical parameters, '$\lambda\rho$,' '$\mu\rho$,' and 'λ/μ' fluid stack from P and S inversion" by Goodway et al. (CSEG 1997 Abstract). "Extracting meaningful geologic parameters using multiple attribute analysis on AVO derived Lamé rock parameter inversions: 3D seismic case study from southern Alberta, Canada" by Pruden (*SEG 2002 Expanded Abstracts*). "Visualizing 3D AVO crossplotting" by Ross and Sparlin (*SEG 2000 Expanded Abstracts*). TLE

Acknowledgments: We gratefully acknowledge the data courtesy extended to us by Kicking Horse Resources Ltd. Calgary. We thank Doug Pruden, GEDCO, Calgary, for the initial interpretation carried out on the data, Jan Dewar for her valuable comments and suggestions, and Joanne Lanteigne for formatting some images. Our special thanks go to Vasudhaven Sudhakar for encouraging this work and Core Laboratories for permisson to publish this paper. Coherence Cube is a trademark of Core Laboratories.

Satinder Chopra is manager, Special Projects with Core Lab Reservoir Technologies, Calgary, and specializes in AVO/LMR analysis, VSP and Coherence Cube processing. He obtained a master's degree (1978) in physics from Himachal Pradesh University, Shimla, India, and worked for more than 13 years for the Oil and Natural Gas Corporation of India. He has 18 years of experience in the field of seismic processing, special processing, and interpretation.

Vladimir Alexeev has a master's degree in geophysics from the Moscow Geological Prospecting Institute. He has 24 years of experience in processing, special processing, and interactive interpretation of seismic data.

Yong Xu is a processing geophysicist and also involved in R&D. He has a master's degree in geophysics from the University of Calgary. He has seven years of experience in AVO processing and migration of seismic data.

Corresponding author: schopra@corelab.ca